The sideslip angle for left-panel stall is reduced to 12 deg by assuming a larger downwash angle than in the calculations for Fig. 1. Changing ε_0 from 4 to 8 deg in Eq. (6) has this effect.

Conclusions

1) V-tail panel geometric angles of attack and sideslip are functions of six variables: airplane angles of attack and sideslip, average downwash and sidewash angles, and V-tail dihedral and incidence.

2) In sample landing approach calculations sideslip angles of 17 deg, possibly reached in turbulence, are calculated to take left V-tail panels with 30 deg of dihedral to the stall point. The stall point is reached at a reduced sideslip angle of 14 deg for a dihedral angle of 40 deg.

3) In sideslip, induction from the opposite panel reduces local panel angles of attack, relative to the case for no sideslip. However, thicker boundary layers caused by crossflow would lead to lower panel stall angles, relative to the case without sideslip.

4) The critical sideslip angle for V-tail panel stall is reduced by 3 deg in the sample case, when the assumed sidewash is increased from 20 to 50% of the sideslip angle. The critical sideslip angle for V-tail stall is reduced to 12 deg when the downwash factor ε_0 is increased from 4 to 8.

References

[1]Purser, P. E., and Campbell, J. P., "Experimental Verification of a Simplified Vee-Tail Theory and Analysis of Available Data on Complete Models with Vee-Tails," NACA Rept. 823, 1945.

[2]McRuer, D. T., Ashkenas, I. L., and Graham, D., *Aircraft Dynamics and Automatic Control*, 1st ed., Princeton Univ. Press, Princeton, NJ, 1973, pp. 224–227.

[3]The Mathworks, Inc., *The Student Edition of MATLAB®, Version 5*, 1st ed., Prentice–Hall, Upper Saddle River, NJ, 1997, pp. 42–46.

Prediction of Laminar/Turbulent Transition in Airfoil Flows

Jeppe Johansen*
Risoe National Laboratory, 4000 Roskilde, Denmark
and
Jens N. Sørensen†
Technical University of Denmark, 2800 Lyngby, Denmark

Nomenclature

C_D	= dissipation coefficient
C_f	= skin-friction coefficient
G_γ	= modeling constant
H	= shape factor
H^*	= kinetic energy shape parameter
Re_c	= Reynolds number based on chord length
Re_x	= Reynolds number based on distance from stagnation point
Re_θ	= Reynolds number based on momentum thickness
$U_\tau = \sqrt{(\tau_w/\rho)}$	= friction velocity
u_e	= velocity at the edge of the boundary layer
x_{tr}	= transition point location
$y^+ = yU_\tau/\nu$	= nondimensional distance from wall
α_i	= imaginary part of spatial wave number
γ	= intermittency function
δ	= boundary-layer thickness
δ_3	= kinetic energy thickness
δ^*	= displacement thickness
θ	= momentum thickness
ν	= viscosity
ξ	= streamwise coordinate
ϕ	= amplitude of perturbation

Presented as Paper 98-0702 at the AIAA 36th Aerospace Sciences Meeting, Reno, NV, 12–15 January 1998; received 6 December 1998; revision received 10 March 1999; accepted for publication 20 March 1999.

*Ph.D. Student, Wind Energy and Atmospheric Physics Department, P.O. Box 49.

†Associate Professor, Department of Energy Engineering.

Introduction

COMPUTATION of flows over airfoils is a challenging problem because of the various complex phenomena connected with the occurrence of separation bubbles and the onset of turbulence. In many engineering applications involving weak streamwise pressure gradients and small curvature effects, turbulent quantities can be predicted well assuming fully turbulent flow. In the case of low-Reynolds-number airfoil flows [$Re < o(10^6)$], proper modeling of the transition point is crucial for predicting leading-edge separation. The transition prediction algorithm must be reliable because the transition point may affect the termination of a transitional separation bubble and hence determine bubble size and associated losses. This again has a strong influence on airfoil characteristics, with drag being the most affected.

A popular transition prediction model is the empirical criterion by Michel.[1] As shown in Refs. 2 and 3, this model gives fairly good results for many airfoil flows. In the present study the more general e^n method, proposed originally by Smith[4] and van Ingen,[5] is compared to the Michel criterion. The e^n method is based on linear stability analysis using the Orr–Sommerfeld equation to determine the growth of spatially developing waves. There have been several attempts by Drela and Giles[6] and Cebeci[7] to apply simplified versions of the e^n method in combination with the viscous-inviscid interaction algorithm.

In the present work a database on stability, with integral boundary-layer parameters as input, has been established. This database avoids the need for computing growth rates for each velocity profile. Furthermore, in order not to determine boundary-layer parameters such as displacement thickness, momentum thickness, and boundary-layer edge velocity using a Navier–Stokes (NS) solver, the NS solver is combined with an integral boundary-layer formulation.

Methods

Flow Solver

The results determined in the present study are computed using EllipSys2D, a general purpose two-dimensional incompressible NS solver, developed by Michelsen[8,9] and Sørensen[10] and based on a multiblock finite volume discretization of the Reynolds averaged NS equations in general curvilinear coordinates. The code uses primitive variables (u, v, and p). The pressure-velocity coupling is obtained with the SIMPLE method by Patankar[11] for steady-state calculations. Solution of the momentum equations is obtained using a second-order upwind scheme. The steady-state calculations are accelerated by the use of local time stepping and a three-level grid sequence.

The turbulence model employed in the present work is the two-equation k–ω SST (shear stress transport) turbulence model by Menter,[12] who obtained good predictions in flows with adverse pressure gradients.

Transition Prediction Models

In the present study two different transition prediction models are used. These are the empirical one-step model of Michel[1] and a semi-empirical e^n model based on linear stability in the form of a database, as suggested by Stock and Degenhart.[13] The Michel criterion is a simple model based on experimental data that correlates local values of momentum thickness with position of the transition point. It simply states that transition takes place where

$$Re_{\theta,\mathrm{tr}} = 2.9Re_{x,\mathrm{tr}}^{0.4} \tag{1}$$

The second model is based on linear stability theory and is referred to as the e^n model by Smith[4] and van Ingen.[5] Linear stability theory suggests that the unperturbed steady and parallel mean flow is superimposed with a time-dependent sinusoidal perturbation—the Tollmien–Schlichting waves. This results in the well-known Orr–Sommerfeld equation, which is a fourth-order linear eigenvalue problem in ϕ. This equation determines whether spatially developing waves will be stable or unstable because of the amplification factor α_i. For positive α_i the waves are damped, and for negative α_i the waves are growing and the flow becomes unstable. In this way the point of instability can be determined. This is defined as where $\alpha_i = 0$, i.e., neutral stability.

The e^n model predicts turbulence when the amplitude of the most unstable frequency exceeds the initial unstable amplitude by a factor e^n. The n factor is empirically determined from several experimental data and can vary from one flow situation to another. It is usually set at a value around 8–10. In the present work it is set at 9, i.e., when the amplitude of the most unstable spatially developing wave has increased by a factor $e^9 \approx 8100$. For further details about the e^n model, see Refs. 4, 5, and 14.

In the present work a database on stability, with integral boundary-layer parameters as input, has been established, as suggested by Stock and Degenhart.[13]

The approach is based on the idea that a discrete set of results to the Orr–Sommerfeld equation is representative for all possible laminar velocity profiles and for all relevant disturbance frequencies. The database consists of stability data on laminar velocity profiles represented by laminar boundary-layer parameters δ^*, θ, δ_3, and u_e. The velocity profiles included in the database vary from velocity profiles with strong favorable pressure gradient to separated velocity profiles. For each of these profiles, a number of frequencies are investigated by solving the Orr–Sommerfeld equation, and the resulting stability data are stored in the database together with the corresponding boundary-layer parameters. The relevant stability information can then be extracted by interpolation.

The database was originally implemented by using Falkner–Skan velocity profiles and has recently been extended to include separated velocity profiles described by hyperbolic tangent functions.

Transition Region

The extension of the transition region is obtained by an empirical model, suggested by Chen and Thyson.[15] This is a conceptually simple model that scales the eddy viscosity by an intermittency function, varying from zero in the laminar region and progressively increases in the transitional region until it reaches unity in the fully turbulent region. The intermittency function, γ_{tr}, is given by

$$\gamma_{\mathrm{tr}}(x) = 1 - \exp\left[\left(-\frac{u_e^3}{\nu^2 G_{\gamma_{\mathrm{tr}}}}\right) Re_{x_{\mathrm{tr}}}^{-1.34}(x - x_{\mathrm{tr}}) \int_{x_{\mathrm{tr}}}^{x} \frac{\mathrm{d}x}{u_e}\right] \tag{2}$$

The modeling constant $G_{\gamma_{\mathrm{tr}}}$ was originally suggested to be 1200 for high-Reynolds-number flows. To take into account separation, especially for low-Reynolds-number flows, it was modified by Cebeci[7] to take the form

$$G_{\gamma_{\mathrm{tr}}} = 213\frac{\log\left(Re_{x_{\mathrm{tr}}}\right) - 4.732}{3} \tag{3}$$

The range at which this modification is valid is $Re_c = 2.4 \times 10^5$ to 2×10^6.

Integral Boundary-Layer Formulation

The input parameters for the database are the laminar boundary-layer parameters δ^*, θ, δ_3, u_e, and Re_c. This results in some difficulties. First, the determination of boundary-layer parameters using the NS solver is not accurate, because the boundary-layer thickness δ is not a trivial parameter to determine. Various attempts include definitions of δ based on vorticity.[16] Second, the turbulence starting from the transition point influences the flow upstream because of the elliptic nature of the flow. This results in boundary-layer parameters differing from their fully laminar value resulting in erroneous interpolation in the database. An alternative procedure is thus required for calculating these parameters. The procedure chosen in the present study solves the integral boundary-layer equations using an NS solver as a boundary condition for freestream velocity. Because the transition procedure should be able to take separation into account, the necessity of an NS solver is clear. The boundary-layer formulation is a two-equation integral model based on dissipation closure. The two equations are the von Karman integral relation given by

$$\frac{\mathrm{d}\theta}{\mathrm{d}\xi} + (2 + H)\frac{\theta}{u_e}\frac{\mathrm{d}u_e}{\mathrm{d}\xi} = \frac{C_f}{2} \tag{4}$$

The second equation is a combination of Eq. (4) and the kinetic energy thickness equation and is given by

$$\theta\frac{\mathrm{d}H^*}{\mathrm{d}\xi} + H^*(1 - H)\frac{\theta}{u_e}\frac{\mathrm{d}u_e}{\mathrm{d}\xi} = 2C_D - H^*\frac{C_f}{2} \tag{5}$$

For laminar flow the two ordinary first-order differential equations can be solved with the following closure relationship for C_f:

$$Re_\theta\frac{C_f}{2} = -0.067 + 0.01977\frac{(7.4 - H)^2}{(H - 1)}, \qquad H < 7.4 \tag{6}$$

together with the additional functional dependencies $H^* = H^*(H, \theta)$ and $C_D = C_D(H, \theta)$. This model has successfully been used by Drela and Giles.[6] To solve Eqs. (4) and (5), a third relation is necessary. By using the NS solver to compute the pressure at the surface and assuming no pressure variation across the boundary layer ($p_{\mathrm{wall}} = p_e$), u_e can be determined from u_∞ using the Bernoulli equation along a streamline. The two equations are then solved by a Newton–Raphson method. Close to the stagnation point, where the skin friction varies dramatically and a small variation in skin-friction factor causes a large variation in edge velocity, the equations are solved using a direct procedure (solve for θ and H, given u_e). When approaching separation, the direct procedure becomes ill-conditioned because a single-edge velocity corresponds to two different skin-friction factors. By computing C_f using the NS solver, H can be computed using the closure relation, Eq. (6), and Eqs. (4) and (5) can be solved inversely with θ and u_e as variables.

Results and Discussion

Two airfoils were tested. The thin NACA0012 airfoil at $Re = 3 \times 10^6$ was chosen as a high-Reynolds-number case, and the 19% thick FX 66-S-196 V1 Wortmann airfoil at $Re = 1.5 \times 10^6$ was chosen where a larger transitional influence should be expected. The computations were carried out assuming steady-state conditions to take advantage of the local time-stepping procedure. For each airfoil a grid-refinement study was carried out resulting in a 288 × 96 grid for both airfoils. The grid spacing to the first gridline off the surface is $y^+ \approx 1$. This ensures that the laminar sublayer is properly resolved.

Figure 1 shows the drag curve for the NACA0012 airfoil, computed with fully turbulent flow and using the two different transition

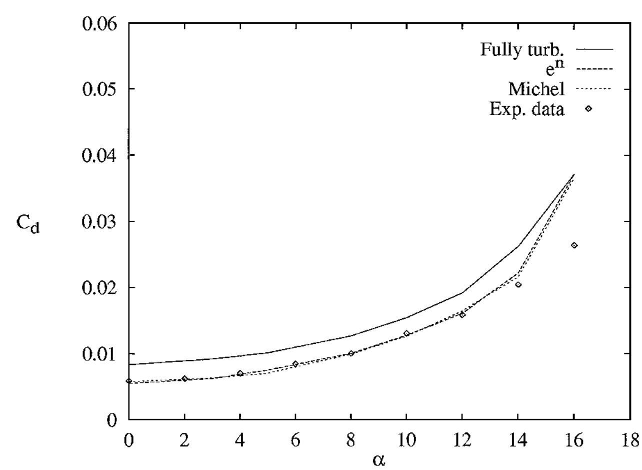

Fig. 1 Drag curve for fully turbulent flow compared with transitional flow and experimental data: NACA0012, $Re = 3 \times 10^6$.

Table 1 Transition point locations for the NACA0012 airfoil at $Re = 3 \times 10^6$

	$x_{tr_{up}}$			$x_{tr_{low}}$		
α	exp	e^n	Michel	exp	e^n	Michel
0	0.45	0.44	0.43	0.45	0.44	0.43
3	0.20	0.19	0.21	0.66	0.68	0.72
5	0.085	0.060	0.13	0.79	0.84	0.88
8	0.024	0.025	0.070	0.92	0.99	1.00
10	0.013	0.014	0.040	1.00	1.00	1.00
12	——	0.012	0.014	1.00	1.00	1.00

Table 2 Transition point locations for the FX 66-S-196 V1 airfoil at $Re = 1.5 \times 10^6$

	$x_{tr_{up}}$			$x_{tr_{low}}$		
α	exp	e^n	Michel	exp	e^n	Michel
−4	——	0.50	0.56	——	0.27	0.25
0	0.53	0.46	0.50	0.50	0.46	0.50
4	0.50	0.45	0.46	0.54	0.50	0.57
8	0.46	0.43	0.40	0.60	0.54	0.73
9	0.45	0.35	0.32	0.62	0.55	0.76
10	0.27	0.17	0.18	0.66	0.57	0.93
11	——	0.11	0.12	——	0.61	1.00
12	——	0.05	0.09	——	0.64	1.00

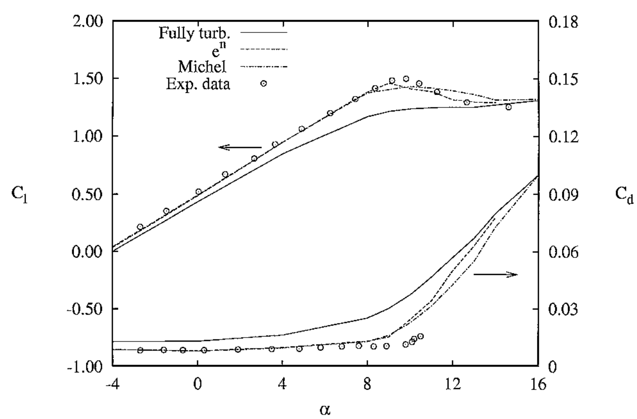

Fig. 2 Lift and drag curves for fully turbulent flow compared with transitional flow and experimental data: FX 66-S-196 V1, $Re = 1.5 \times 10^6$.

prediction models compared with experimental data.[17] A better prediction is obtained for the drag using the transition models. This emphasizes the importance of transition point prediction when computing drag characteristics. The pressure distribution is hardly influenced, indicating that the computed lift coefficients were almost unaffected. There is no significant difference between the two transition models.

In Table 1 computed transition point locations are compared with experimental data.[17] For small angles of attack both models exhibit good agreement with experimental data. For higher angles of attack ($\alpha > 5$ deg) the e^n model gives a better prediction of the location of the transition point. The transition point predicted by the Michel criterion showed a more fluctuating behavior than that predicted by the e^n model, resulting in larger fluctuations in lift and drag coefficients. The transition point predicted using the e^n model stabilized in just a few iterations, and the converged solution was obtained faster.

The lift and drag curves of the 19% thick FX 66-S-196 V1 airfoil are shown in Figure 2, compared with experimental data.[18] The fully turbulent computation is obviously unacceptable; using the transition prediction models gives better results. Both models predict lift and drag well up to maximum lift, but at light stall the models predict transition before the experimentally determined value. At high angles of attack, the transition point approaches the leading edge, i.e., the lift approaches the fully turbulent computation. The computed transition points are shown in Table 2, and both models give comparable predictions. Again using the Michel criterion resulted in a fluctuating transition point location leading to a longer convergence time.

Conclusions

This study has described the coupling of a simplified version of the e^n transition model together with an NS solver applied to low-Reynolds-number airfoil flows. A two-equation integral laminar boundary-layer formulation was solved using a coupled direct/inverse formulation to determine laminar integral boundary-layer parameters. The inverse procedure was chosen to obtain integral parameters well into the separated region, and also to overcome the difficulty of defining the velocity at the edge of the boundary layer. Comparisons with the simple empirical Michel criterion and with experimentally determined transition point locations were made.

The results obtained in the present study indicate that proper transition point prediction is crucial, especially when considering the drag characteristics.

The NACA0012 airfoil at $Re = 3 \times 10^6$ has only a minor effect on the lift prediction, whereas the drag characteristics are influenced to a greater extent. The FX 66-S-196 V1 airfoil at $Re = 1.5 \times 10^6$ clearly shows the importance of transition prediction for both lift and drag characteristics.

No particular difference in integrated flow characteristics was obtained between the two models, but a faster convergence was obtained using the e^n model caused by stable transition point location. This model is thus superior to the empirical model and is therefore preferable.

References

[1] Michel, R., "Etude de la Transition sur les Profiles d'Aile; Etablissement d'un Critére de Determination de Point de Transition et Calcul de la Trainee de Profile Incompressible," ONERA, TR, Rept. 1/1578A, Toulouse, France, 1951.

[2] Ekaterinaris, J. A., Chandrasekhara, M. S., and Platzer, M. F., "Analysis of Low Reynolds Number Airfoil Flows," *Journal of Aircraft*, Vol. 32, No. 3, 1995, pp. 625–630.

[3] Mehta, U., Chang, K. C., and Cebeci, T., "Relative Advantages of Thin-Layer Navier–Stokes and Interactive Boundary-Layer Procedures," NASA, TM86778, Nov. 1985.

[4] Smith, A. M. O., "Transition, Pressure Gradient, and Stability Theory," *Proceedings of the IX International Congress of Applied Mechanics*, Vol. 4, 1956, pp. 234–244.

[5] Van Ingen, J. L., "A Suggested Semi-Empirical Method for the Calculation of the Boundary-Layer Region," Dept. of Aerospace Engineering, Technical Univ. of Holland, TR VTH71, VTH74, Delft, Holland, 1956.

[6] Drela, M., and Giles, M. B., "Viscous-Inviscid Analysis of Transonic and Low Reynolds Number Airfoils," *AIAA Journal*, Vol. 25, No. 10, 1986, pp. 1347–1354.

[7] Cebeci, T., "Essential Ingredients of a Method for Low Reynolds-Number Airfoils," *AIAA Journal*, Vol. 27, No. 12, 1988, pp. 1680–1688.

[8] Michelsen, J. A., "Basis 3D—a Platform for Development of Multiblock PDE Solvers," Technical Univ. of Denmark, TR AFM 92-05, Lyngby, Denmark, Dec. 1992.

[9] Michelsen, J. A., "Block Structured Multigrid Solution of 2D and 3D Elliptic PDE's," Technical Univ. of Denmark, TR AFM 94-06, Lyngby, Denmark, May 1994.

[10] Sørensen, N. N., "General Purpose Flow Solver Applied to Flow over Hills," Risø National Lab., Risø-R-827-(EN), Roskilde, Denmark, June 1995.

[11] Patankar, S. V., *Numerical Heat Transfer and Fluid Flow*, Hemisphere, New York, 1980, pp. 126–131.

[12] Menter, F. R., "Zonal Two Equation k–ω Turbulence Models for Aerodynamic Flows," AIAA Paper 93-2906, July 1993.

[13] Stock, H. W., and Degenhart, E., "A Simplified e^n Method for Transition Prediction in Two-Dimensional, Incompressible Boundary Layers," *Zeitschrift für Flugwlssenschaften*, Vol. 13, No. 13, 1989, pp. 16–30.

[14] Arnal, D., "Boundary Layer Transition: Predictions Based on Linear Theory," TR, AGARD-R-793, AGARD, Neuilly-sur-Seine, France, 1994.

[15] Chen, K. K., and Thyson, N. A., "Extension of Emmons Spot Theory to Flows on Blunt Bodies," *AIAA Journal*, Vol. 9, No. 5, 1971, pp. 821–825.

[16] Spalart, P. R., and Watmuff, J. H., "Experimental and Numerical Study of a Turbulent Boundary Layer with Pressure Gradient," *Journal of Fluid Mechanics*, Vol. 249, April 1993, pp. 337–371.

[17]Gregory, N., and O'Reilly, C. L., "Low-Speed Aerodynamic Characteristics of NACA0012 Airfoil Section, Including the Effects of Upper-Surface Roughness Simulating Hoar Frost," TR, NPL AERO Rept. 1308, Middlesex, England, UK, 1970.

[18]Althaus, D., and Wortmann, F. X., "Stuttgarter Profilkatalog I," Technical Rept., F. Vieweg-Verlagsgesellschaft m.b.H., Braunschweig, Germany, 1981.

Best-Range Altitude for Jet-Propelled Aircraft

Miguel Angel Gómez-Tierno,*
Juan José Martínez-García,† and Manuel Pérez-Cortés‡
Universidad Politécnica de Madrid,
28040 Madrid, Spain

Nomenclature

$C_{L\text{opt}}$ = lift coefficient for $E_{\max}$
c = specific fuel consumption
$E_{\max}$ = maximum aerodynamic efficiency for parabolic polar
h = altitude, m
S = wing area
T = thrust
t = dimensionless thrust, $(TE_{\max}/W)$
V = airspeed
V_R = reference or minimum drag airspeed, $(2W/\rho SC_{L\text{opt}})^{1/2}$
v = dimensionless airspeed, V/V_R
W = aircraft weight
W_F = fuel weight
X = range
X_R = reference range, $\{8V_{Ri0}E_{\max}[1-(1-\zeta)^{1/2}]\}/(c_{11}\sigma_{11}^{0.5})$
y = dimensionless exponent for specific fuel consumption
z = dimensionless exponent for thrust
ζ = fuel-to-initial-weight ratio, W_F/W_i
ρ = air density
σ = relative air density with respect to sea level, ρ/ρ_0

Subscripts

a = flight condition for v equal to $3^{1/4}$
br = best (maximum) range condition
c = absolute ceiling condition (based on initial weight)
i = initial weight condition
m = maximum thrust condition
0 = sea level, 0 m
11 = tropopause level, 11,000 m

Introduction

In classical flight mechanics,[1–3] the range of a jet-propelled aircraft is calculated using simplified assumptions about aerodynamic characteristics, e.g., parabolic polar, no compressibility effects; engines, e.g., thrust and specific fuel consumption are proportional to powers of air density; and flight profiles, e.g., quasisteady and level flight. For a given altitude, the maximum range with a constant altitude–constant lift coefficient flight program is achieved with dimensionless airspeed constant and equal to $3^{1/4}$. When increasing altitude to maximize this maximum range, two problems appear: First, exponents fitting thrust and specific fuel consumption as powers of the air densities are different in the troposphere and stratosphere and different models must be used in those layers. Second, the available thrust has a finite maximum value and is impossible to fly at $v = 3^{1/4}$ above certain altitude. This Note analytically solves these problems, offers a closed formulation for the best range and best-range altitude, and compares them with the ceiling range and ceiling altitude.

Basic Equations

The usual approaches for thrust and specific fuel consumption of a jet engine are

$$t/t_{11} = (\sigma/\sigma_{11})^z, \qquad c/c_{11} = (\sigma/\sigma_{11})^y \tag{1}$$

where t_{11} depends on thrust setting and c_{11} is a constant.

The quasisteady level flight condition for an aircraft with a parabolic polar gives a relationship between t and v,

$$t = \tfrac{1}{2}[v^2 + (1/v^2)] \tag{2}$$

The well-known range equation for a jet-propelled aircraft with constant altitude–constant lift coefficient flight program is[1–3]

$$X = \frac{4V_{Ri0}E_{\max}(1-\sqrt{1-\zeta})\sigma_{11}^y}{c_{11}}\frac{1}{\sigma^{y+0.5}}\frac{v^3}{v^4+1} \tag{3}$$

and the classical unconstrained best-range condition for a fixed altitude (or fixed σ) is

$$v = 3^{\frac{1}{4}} = 1.316, \qquad t = 2/3^{\frac{1}{2}} = 1.155$$

Thus,

$$X_a = \frac{3^{\frac{3}{4}}V_{Ri0}E_{\max}(1-\sqrt{1-\zeta})\sigma_{11}^y}{c_{11}}\frac{1}{\sigma^{y+0.5}}$$

The preceding expression increases as σ decreases (that is, as altitude increases), and the maximum value for best range would be reached at the absolute ceiling. At the absolute ceiling, however, the only possible airspeed is $v = 1$ [and consequently, by means of Eq. (2), $t = 1$]. Therefore, it is necessary to change the formulation to analyze the dimensionless interval $1 \le v \le 1.316$, with the constraint that in any point of the trajectory the thrust must be lesser or equal to the maximum available thrust ($T \le T_m$).

Additional problems arise due to the different exponents z and y used in the troposphere and stratosphere. Typical values for a turbojet are[1] troposphere: $z = 0.7$ and $y = 0.2$ and stratosphere: $z = 1.0$ and $y = 0$. Using these values, two separate formulations for the troposphere and stratosphere are proposed.

Troposphere ($z = 0.7, y = 0.2$)

By the changing of the two degrees of freedom, from v and σ to v and t_{11}, Eq. (3) is transformed to

$$X = \frac{8V_{Ri0}E_{\max}(1-\sqrt{1-\zeta})}{c_{11}\sigma_{11}^{0.5}}t_{11}\frac{v^5}{(v^4+1)^2}$$

By the use of a reference range defined as

$$X_R = \frac{8V_{Ri0}E_{\max}(1-\sqrt{1-\zeta})}{c_{11}\sigma_{11}^{0.5}}$$

a condensed expression for the range is obtained

$$\frac{X}{X_R} = t_{11}\frac{v^5}{(v^4+1)^2} \tag{4}$$

where $t_{11} = T_{11}E_{\max}/W$ is maintained constant in the flight.

For the best-range condition, Eq. (4) has a maximum for

$$t_{11\text{br}} = t_{11mi} = (T_{11m}/W_i)E_{\max}, \qquad v_{\text{br}} = \left(\tfrac{5}{3}\right)^{\frac{1}{4}} = 1.136$$

Therefore, $t_{\text{br}} = 4/15^{1/2} = 1.033$, $\sigma_{\text{br}}/\sigma_{11} = (1.033/t_{11mi})^{1/0.7}$, and $X_{\text{br}}/X_R = 0.2663 \times t_{11mi}$.

Received 18 January 1999; revision received 10 March 1999; accepted for publication 20 March 1999.

*Associate Professor of Flight Mechanics, E.T.S. Ingenieros Aeronáuticos. Member AIAA.

†Professor of Flight Mechanics, E.T.S. Ingenieros Aeronáuticos. Member AIAA.

‡Associate Professor of Flight Mechanics, E.T.S. Ingenieros Aeronáuticos, Departamento de Vehículos Aeroespaciales, Plaza Cardenal Cisneros, 3.